Low Temperature Physics/Fizika Nizkikh Temperatur, 2021, vol. 47, No. 7, pp. 602–612

Dynamical Green's function for elastic half-space, and energy losses due to collision

Marina Litinskaya

Department of Physics and Astronomy, University of British Columbia, Vancouver V6T 1Z1, Canada
E-mail: litinskaya@gmail.com

Inna Kaganova

Center of Optical Neural Technologies, Scientific Research Institute for System Analysis RAS
Moscow 117218, Russia
E-mail: imkaganova@gmail.com

Received March 10, 2021, published online May 26, 2021

This special issue celebrates 100 years since the birth of Moisey Isaakovich Kaganov. This date is a personal event for us, since Moisey Issakovich (or Musik, for his friends and close ones) is the father of one of us, and the grandfather of the other. In addition, we have both been his students. We received the problem discussed in this paper by succession. In 1949 Ilya Mikhailovich Lifshitz was interested in studying electrodynamic and elastic properties of solids, and this analysis required knowledge of the corresponding Green's functions. He suggested to his two graduate students, Moisey Kaganov and Victor Tzukernik, to calculate the displacement vector caused by an instant point source acting at the surface of an elastic half-space. At that time they had chosen a different topic, and the problem hibernated until the early 1990s, when Moisey Issakovich suggested it as a subject for a Master's thesis for one of us (ML) to be conducted under the supervision of the other one (IK). The results have been published in papers I. M. Kaganova and M. L. Litinskaia, *Phys. Lett. A* **200**, 365 (1995) [1] and I. M. Kaganova and M. L. Litinskaia, *Phys. Lett. A* **200**, 375 (1995) [2]. The first paper discussed the derivation of the normal component of the displacement vector. We showed that the displacement can be calculated as an integral in the complex plane, and examined the displacement at the surface of the half-space and at the direction normal to the surface. We showed that the singularities of the displacement are linked to certain changes in the shape of the integration contour. In the second paper, we applied the expression for the normal displacement to the calculation of the elastic energy due to an external load, and found the amount of energy lost by a small ball incident onto an elastic half-space. In this publication, we expand the analysis by investigating the singularities of the displacement vector in an arbitrary point of the half-space, and briefly review our previous results.

Keywords: Green's functions, elastic half-space, displacement vector, integration contour shape.

1. Introduction

Propagation of sound waves in elastic media has been studied since long ago. Applications include a wide range of solid state physics problems, applied problems and seismological disturbances. To find the waves excited in an elastic medium by an external load it is often convenient to use the Green's function, which describes the response of the medium to a point-like momentarily load. Then the elastic response to a spatially distributed and time-dependent source can be calculated by convoluting the Green's function and the load.

As known [3], elastic media support various kinds of waves. Firstly, in an infinite medium there are longitudinal and transverse waves, which are coupled by elastic dynamical equations, and cannot be treated independently. Secondly, if the geometry of the problem assumes presence of a boundary, the system supports additional surface modes. In an elastic half-space these modes are known as Rayleigh waves. Each component of the displacement vector is a wave packet made of all the tree types of the waves, and its specific form is dictated by the boundary conditions and the external load. A naive glance into what this vector might look like for a half-space subject to delta-like source suggests

emergence of a non-trivial pattern possibly featured by presence of singularities. Indeed, the Green's function for the simplest scalar wave equation,

$$c^2\Delta U - d^2U/dt^2 = A\delta(\mathbf{r})\delta(t),$$

crucially depends on the dimensionality of the problem: while in 3D the displacement $U_{3D} \propto \delta(r-tc)/r$ is a sphere with a zero distortion inside it and a delta-like singularity at the wave front, in 2D the displacement U_{2D} exists for all $r < tc$, and has another singularity at the wave front: it diverges as $U_{2D}(r \to tc) \sim 1/\sqrt{(tc)^2 - r^2}$. In a semi-infinite medium the bulk waves, which might be similar to U_{3D}, will coexist with 2D-like surface Rayleigh waves, which might be similar to U_{2D}. These qualitative arguments hint at a possible presence of delta-like singularities and interplay between "empty" (zero-distortion) and "filled" (finite distortion) tendencies.

The presence of a surface makes the problem less tractable than in an infinite system. Before [1], only asymptotic expressions for the displacement vector, which hold at the distances large comparatively to the size of the source, were known [4]. Below, following [1], we derive the expression for the dynamical Green's function for a semi-infinite elastic medium. After that, we analytically investigate the locus of its singularities and discontinuities, which are of special interest. We use complex analysis to connect these peculiar points with the dynamics of the singularities in the Green's function integral representation (Sec. 2). Specifically, delta-like singularities and jumps of the displacement vector appear when a pair of time- and position-dependent singularities overlaps with one of the "stationary" singularities determined solely by the elastic constants of the medium. In Sec. 3 following [2], we study the elastic energy associated with the displacement caused by a point-like surface force and by a distributed load, for example, by a small ball incident on the surface of the half-space. We show that the major part of the elastic energy is carried by the surface waves. Our results can be used in many theoretical and applied problems of classical theory of elasticity, as well as for studying interaction between particles and solid medium: though such problems require quantum-mechanical consideration, knowing the classical limit may appear to be useful.

2. Dynamical Green's function

2.1. General equations

We consider a semi-infinite solid medium, which occupies the half-space $x_3 > 0$. The components of the displacement vector **u**, which describes elastic waves in this medium, satisfy the dynamical equation

$$\rho \frac{\partial^2 u_i}{\partial t^2} = \frac{\partial \sigma_{ik}}{\partial x_k}, \tag{1}$$

where ρ is the density of the medium, and σ_{ik} are the components of the stress tensor, which obey the Hooke law

$$\sigma_{ik} = 2\rho c_t^2 u_{ik} + \rho(c_l^2 - 2c_t^2)u_{ll}\delta_{ik}, \quad u_{ik} = \frac{1}{2}\left(\frac{\partial u_i}{\partial x_k} + \frac{\partial u_k}{\partial x_i}\right), \tag{2}$$

where c_l and c_t are, respectively, the longitudinal and transverse speed of sound (as known, $c_l > c_t$). Here and below summation over repeated indexes is assumed.

Let an instantaneous force with a magnitude F act at $t = 0$ at the point $x_1 = x_2 = 0$ normally to the surface: $\mathbf{F} = (0, 0, F\delta(\mathbf{r}_\parallel)\delta(t))$, with $\mathbf{r}_\parallel$ being a radius-vector in the (x_1, x_2)-plane. Then the boundary conditions for the elastic system can be written as

$$\sigma_{31}(x_3 = 0) = \sigma_{32}(x_3 = 0) = 0, \quad \sigma_{33}(x_3 = 0) = F\delta(\mathbf{r}_\parallel)\delta(t). \tag{3}$$

The displacement vector that satisfies Eqs. (1)–(3) is the Green's function of the elastic half-space. We denote it as $\mathbf{U}(\mathbf{r}_\parallel, x_3; t)$, Fourier transform its components

$$U_i(\mathbf{r}_\parallel, x_3; t) = \int_{-\infty}^{\infty} d\omega e^{-i\omega t} \int d\mathbf{k}_\parallel e^{i(\mathbf{k}_\parallel \mathbf{r}_\parallel - \omega t)} V_i(\mathbf{k}_\parallel, \omega; x_3), \tag{4}$$

and set up the system of equations for its Fourier coefficients $V_i(\mathbf{k}_\parallel, \omega; x_3)$. This problem has been solved in [5] for an arbitrary direction of the applied force. For the normal surface force the components of the displacement vector $\mathbf{U}(\mathbf{r}_\parallel, x_3; t) = \left(U_\parallel(r_\parallel, x_3; t), 0, U_3(r_\parallel, x_3; t)\right)$ written in cylindrical coordinates become:

$$U_\parallel(r_\parallel, x_3; t) = -\frac{F}{\rho c_t^2 (2\pi)^2} \int_{-\infty}^{\infty} d\omega\, e^{-i\omega t} \int_0^{\infty} dk_\parallel \frac{k_\parallel^2 J_1(k_\parallel r_\parallel)}{r(k_\parallel^2)} \left[(\alpha_t^2 + k_\parallel^2)\, e^{-\alpha_l x_3} - 2\alpha_l \alpha_t e^{-\alpha_t x_3} \right],$$

$$U_3(r_\parallel, x_3; t) = -\frac{F}{\rho c_t^2 (2\pi)^2} \int_{-\infty}^{\infty} d\omega\, e^{-i\omega t} \int_0^{\infty} dk_\parallel \frac{k_\parallel \alpha_l J_0(k_\parallel r_\parallel)}{r(k_\parallel^2)} \left[(\alpha_t^2 + k_\parallel^2)\, e^{-\alpha_l x_3} - 2k_\parallel^2 e^{-\alpha_t x_3} \right], \tag{5}$$

where $J_{0,1}(x)$ are Bessel functions. The functions

$$\alpha_{l,t}(k_\parallel,\omega)=\begin{cases}\sqrt{k_\parallel^2-\omega^2/c_{l,t}^2}, & k_\parallel>|\omega|/c_{l,t},\\ -i\,\mathrm{sgn}\,(\omega)\sqrt{\omega^2/c_{l,t}^2-k_\parallel^2}, & k_\parallel<|\omega|/c_{l,t}\end{cases} \quad (6)$$

are the normal components of the k-vector of the modes. The sign in front of the square root is chosen so that the excited waves propagate away from the surface. Equations (5) show that the components of the displacement vector are sums of two terms, the first corresponds to longitudinal sound waves (l-waves, $\propto e^{-\alpha_l x_3}$), the second to transverse sound waves (t-waves, $\propto e^{-\alpha_t x_3}$). These two waves are coupled and cannot propagate independently. From Eq. (6) it follows that the range of $k_\parallel$ is naturally divided into three intervals [see Fig. 1(a)] according to the character, either bulk or surface, of the excited waves in each of these two terms.

Furthermore, the denominator of the integrands

$$r(k_\parallel^2)=(\alpha_t^2+k_\parallel^2)^2-4k_\parallel^2\alpha_l\alpha_t \quad (7)$$

has a single root

$$k_\parallel^2=\frac{\omega^2}{c_t^2\xi^2}, \quad (8)$$

which is the dispersion equation for surface Rayleigh waves. Here $\xi=\xi(c_t/c_l)$ is the smallest positive real root of the equation $\xi^6-8\xi^4+8\xi^2(3-2c_t^2/c_l^2)-16(1-c_t^2/c_l^2)=0$, $0.874<\xi<0.955$ [3]. Account of dissipation yields a complex correction to this pole. For infinitesimally small damping, $k_\parallel^2=\omega^2/c_t^2\xi^2+i\delta\,\mathrm{sgn}\,[\omega]$, where $\delta\to+0$.

There are three characteristic sound wave speeds in this problem: $c_t\xi<c_t<c_l$, where $c_t\xi$ is the speed of surface Rayleigh waves. The displacement at a distance R from the origin at a moment t is determined by the superposition of the waves that have reached this point by that time. We introduce a dimensionless parameter

$$\lambda=\frac{tc_l}{R},\quad R=\sqrt{r_\parallel^2+x_3^2}, \quad (9)$$

whose magnitude determines which kinds of waves cause the displacement at point $r_\parallel=R\sin\theta$, $x_3=R\cos\theta$ at a given time t (here θ is the angle counted from the x_3-axis). Figure 1(b) shows characteristic values of the parameter λ, that serve as "boundaries" between various types of waves, and the correspondence between (R,t)- and λ-representations. For example, at $\lambda<1$ (or, equivalently, at $R>c_lt$) the displacement must be zero, since even the fastest longitudinal waves could not reach these locations in time t.

Below we investigate the normal component of the displacement vector, $U_3(r_\parallel,x_3;t)$. The radial component of the displacement vector can be addressed in a similar way. Let us simplify the double integral from Eq. (5). We introduce the shortcuts

$$C_1=\frac{c_l^2}{c_t^2},\quad C_2=\frac{c_l^2}{\xi^2c_t^2} \quad (10)$$

(note that $1<C_1<C_2$) and a dimensionless variable

$$x=\frac{k_\parallel^2}{\omega^2/c_l^2}. \quad (11)$$

As a result of the replacement (11), an extra ω appears in the integral over $d\omega$ in (5). We absorb it into a derivative over time:

$$\int_{-\infty}^{\infty}d\omega\,\omega\,e^{-i\omega t}J_0\left(\omega\frac{r_\parallel\sqrt{x}}{c_l}\right)=-2\,\mathrm{Im}\,\frac{\partial}{\partial t}\int_0^{\infty}d\omega\,e^{i\omega t}J_0\left(\omega\frac{r_\parallel\sqrt{x}}{c_l}\right). \quad (12)$$

Then integration over ω can be carried out using the equality

$$\int_0^{\infty}d\omega\,e^{i\omega t}\,J_0\left(\omega\frac{r_\parallel\sqrt{x}}{c_l}\right)=$$
$$=\frac{\Theta(r_\parallel\sqrt{x}/c_l-t)}{\sqrt{(r_\parallel\sqrt{x}/c_l)^2-t^2}}+i\frac{\Theta(t-r_\parallel\sqrt{x}/c_l)}{\sqrt{t^2-(r_\parallel\sqrt{x}/c_l)^2}}, \quad (13)$$

where $\Theta(x)$ is the Heaviside step function [6]. We can finally write:

$$U_3(R,\lambda,\theta)=\frac{F}{(2\pi)^2\rho}\frac{c_l}{R^2c_t^2}\frac{\partial}{\partial\lambda}\phi(\lambda,\theta), \quad (14)$$

where the function $\phi(\lambda,\theta)$ is the integral over x. It is convenient to split it into two integrals corresponding to the longitudinal and the transverse waves:

$$\phi(\lambda,\theta)\equiv J_l(\lambda,\theta)+J_t(\lambda,\theta). \quad (15)$$

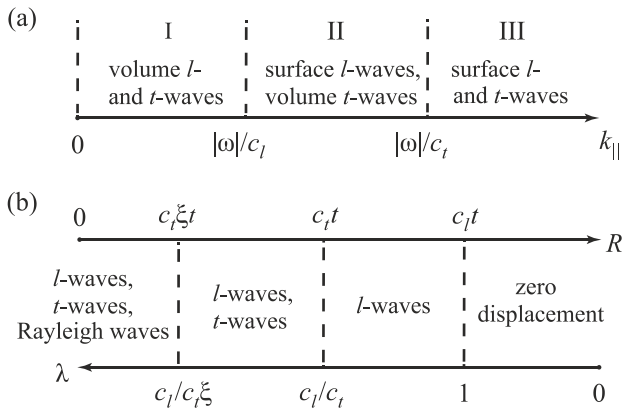

Fig. 1. (a) Three intervals of the wave vector $k_\parallel$, and the type (surface or volume) of longitudinal and transverse waves in each interval. (b) Upper axis shows characteristic distances $R=c_t\xi t, c_t t, c_l t$. For a given time t, these distances set the boundaries of four space regions. Each region is characterized by a specific set of waves (surface Rayleigh waves, transverse, longitudinal, or none of them) that have been able to reach that region. Lower axis: the same four regions in terms of the dimensionless parameter λ (9), which combines temporal and spatial coordinates.

Since, by virtue of (6) and (13), the integrands of $J_l(\lambda,\theta)$ and $J_t(\lambda,\theta)$ have different functional forms in each of the x-intervals shown in Fig. 1(a), it is convenient to write them as follows:

$$J_l(\lambda,\theta) = \int_0^1 dx\ f_l(x;\lambda,\theta)\,\Theta\left(\sqrt{x}\sin\theta - |\,\lambda - \cos\theta\sqrt{1-x}\,|\right) + \\ + \mathrm{Im}\int_1^\infty dx\ f_l(x;\lambda,\theta);$$

$$J_t(\lambda,\theta) = \int_0^1 dx\ f_t(x;\lambda,\theta)\Theta\left(\sqrt{x}\sin\theta - |\,\lambda - \cos\theta\sqrt{C_1-x}\,|\right) + \\ + \mathrm{Im}\int_1^{C_1} dx\ f_t(x;\lambda,\theta)\Big[\Theta\left(\sqrt{x}\sin\theta - |\,\lambda - \cos\theta\sqrt{C_1-x}\,|\right) + \\ + i\,\mathrm{sgn}\left[\lambda - \cos\theta\sqrt{C_1-x}\right]\Theta\left(|\,\lambda - \cos\theta\sqrt{C_1-x}\,| - \sqrt{x}\sin\theta\right)\Big] + \\ + \mathrm{Im}\int_{C_1}^\infty dx\ f_t(x;\lambda,\theta). \tag{16}$$

Here

$$f_l(x;\lambda,\theta) = -\frac{\sqrt{|\,x-1\,|}(2x-C_1)}{\tilde{r}(x)N_l(x;\lambda,\theta)}, \\ f_t(x;\lambda,\theta) = \frac{2x\sqrt{|\,x-1\,|}}{\tilde{r}(x)N_t(x;\lambda,\theta)}, \tag{17}$$

where $\tilde{r}(x)$ is the dimensionless version of the denominator (7), and

$$N_l(x;\lambda,\theta) = \left\{\left(\sqrt{1-a_-} - \sqrt{1-x}\right)\times \right. \\ \left.\times\left(\sqrt{1-x} - \mathrm{sgn}\,(\lambda-\sin\theta)\sqrt{1-a_+}\right)\right\}^{1/2}, \\ N_t(x;\lambda,\theta) = \left\{\left(\sqrt{C_1-b_-} - \sqrt{C_1-x}\right)\times \right. \\ \left.\times\left(\sqrt{C_1-x} - \mathrm{sgn}\,(\lambda-\sqrt{C_1}\sin\theta)\sqrt{C_1-b_+}\right)\right\}^{1/2}, \tag{18}$$

with

$$a_\pm = (\lambda\sin\theta \pm \cos\theta\sqrt{1-\lambda^2})^2 = \\ = [\lambda^2(\sin^2\theta - \cos^2\theta) + \cos^2\theta] \mp 2i\lambda\sqrt{\lambda^2-1}\sin\theta\cos\theta, \\ b_\pm = (\lambda\sin\theta \pm \cos\theta\sqrt{C_1-\lambda^2})^2 = \\ = [\lambda^2(\sin^2\theta - \cos^2\theta) + C_1\cos^2\theta] \mp 2i\lambda\sqrt{\lambda^2-C_1}\sin\theta\cos\theta. \tag{19}$$

For two directions, on the axis x_3 and on the surface $x_3 = 0$, the integrals (16) can be calculated analytically, and the expression for the normal displacement can be obtained by differentiating the result with respect to λ [see Eq. (14)]. We have done this in [1] and found that the answers, while being the limiting cases of the same expression, were astoundingly different. The displacement on the axis x_3 had one delta-singularity, and in this aspect it was similar to a 3D Green's function (see Introduction). Furthermore, it carried no dependence on the Rayleigh wave parameter ξ. In contrast, on the surface the displacement had discontinuities, and it diverged at the Rayleigh wavefront, as is typical for a 2D Green's function.

For an arbitrary direction the integrals (16) cannot be calculated analytically. However, using complex analysis, we can examine the singularities (jumps and cusps) of these two integrals, and hence determine the locus and type (delta-singularities and jumps) of the normal displacement singularities, thus visualizing the wavefront of the signal in the half-space. We do this in the next section.

2.2. Singularities of the dynamical Green's function

We examine the integrals $J_{l,t}(\lambda,\theta)$ (16) by replacing a real x with a complex z and performing contour integration. We find that the singularities of the Green's function of an elastic half-space are entirely determined by the shape of the integration contours, and therefore by the number and mutual locations of the singularities of the integrands of $J_{l,t}(\lambda,\theta)$.

Let us start with identifying the singularities of the integrands of $J_{l,t}(\lambda,\theta)$. Already from Eqs. (6) and (7) it is seen that the function $r(z)$ has three singular points, which are inherited by the integrands: two branch points $z = 1$ and $z = C_1$ (they appear from the square roots in the expressions for $\alpha_{l,t}$) and the Rayleigh pole $z = C_2$ [see Eq. (8)]. These singular points do not depend on the value of the parameter λ, so we will call them "Fixed singularities" (FS). In addition, the integration over ω brings the functions $N_{l,t}(x,\lambda,\theta)$ [see (18)] into the integrands. These functions introduce four additional singularities, $a_\pm(\lambda,\theta)$ and $b_\pm(\lambda,\theta)$ (19). In general, they are four branch points. However, their characters and even their number depend on λ and θ. For example, for small $\lambda < \sin\theta$ there are only two additional branch points, a_- and b_-, while for $\sin\theta < \lambda < \sqrt{C_1}\sin\theta$ we have three additional branch points a_-, a_+ and b_- (see Figs. 3 and 4 below). We will also see that pairs of these branch points can overlap and produce new poles. Since these points depend on λ and θ (i.e., on time and location), we will call them "Moving singularities" (MS).

Assume that θ is fixed, and let λ vary from zero to infinity. This can be viewed as if we have picked an observation point at a distance R from the origin, which has the coordinates $(R\sin\theta, R\cos\theta)$, and look at the displacement at this point as the time goes from $t = 0$ to $t = \infty$. As λ varies, the MS travel around FS, and the shapes of the integration contours for J_l and J_t change accordingly. Certain changes in the shape of the integration contours result in cusps or jumps in the corresponding integral $J_l(\lambda,\theta)$ or $J_t(\lambda,\theta)$ (16). Since, in accordance with Eq. (14), the normal displacement U_3 is the derivative of these integrals over λ, it means that at these values of λ and θ the displacement vector will have, respectively, a jump and a delta-singularity.

Our analysis shows that the singularities of the displacement vector appear as a result of the following events:

– Coincidence of two MS. For small λ the MS are at the real axis. At certain values of (λ,θ) they overlap, i.e., $a_+ = a_-$, or $b_+ = b_-$. Then instead of two branch points a new pole appears in the integrand of, respectively, J_l or J_t. This results in a jump of the corresponding integral and in a delta-like singularity of the displacement.

– An MS-pair moves over a stationary branch point. As we will discuss shortly, and as can be seen from the second form of Eqs. (19), with the increase of λ the pairs of MS (a_+ and a_-, or b_+ and b_-) move away from the real axis and form a pair, which is symmetric about $\mathrm{Re}[z]$-axis (a "vertical pair"). When such a "vertical pair" overlaps with a stationary branch point $x = 1$ or $x = C_1$ (i.e., when $\mathrm{Re}[a_\pm] = 1$ or C_1, and the same for $\mathrm{Re}[b_\pm]$), the corresponding integral J_l or J_t has a cusp. As a result, the displacement has a jump.

– An MS-pair moves over a stationary Rayleigh pole. Finally, at certain values of (λ,θ) a "vertical pair" of MS moves over the Rayleigh pole in the complex plane (it happens when $\mathrm{Re}[a_\pm] = C_2$ or $\mathrm{Re}[b_\pm] = C_2$). This results in a jump of the corresponding integral J_l or J_t, and hence in a delta-like singularity of the displacement.

For all other types of unusual behavior of MS (such as, for example, overlap of a single moving singularity a_+ with a stationary branch point $x = 1$) the integrals J_l or J_t remain regular. Therefore, the singularities of the displacement vector are exhausted by the mentioned events. The magnitude of the displacement between the singular points can be calculated by numerical evaluation of J_l and J_t (16).

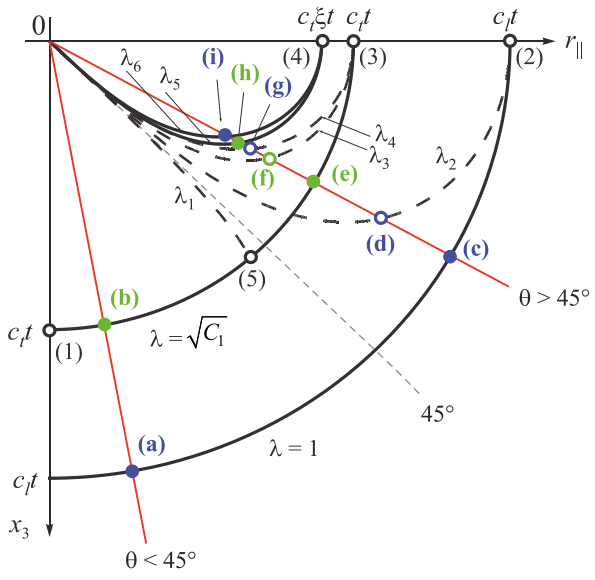

Fig. 2. (Color online) Locations of the Green's function singularities at a fixed moment of time t: delta-singularities are shown by thick solid lines, and discontinuities by thick dashed lines. The black empty circles numbered from 1 to 5 mark the points where the delta-singularities are suppressed. Points marked (a) through (i) connect this diagram with the dynamics of the MS shown in Figs. 3, 4, with blue and green colors referring, respectively, to the MS of the integral J_l and J_t (see text).

The loci of the singularities of the normal displacement are summarized on the diagram in Fig. 2, which shows a snapshot of $U_3(R,\theta;t)$ at some moment t. Thick black solid lines represent delta-singularities, and thick black dashed lines are the lines of the jumps of $U_3(R,\theta;t)$. At some locations shown by black empty circles the magnitude of the jump of J_l or J_t appears to be equal to zero (see below), and the corresponding delta-singularity becomes suppressed. This figure confirms that the displacement near the vertical axis differs dramatically from the displacement near the surface. Indeed, we will see that surface Rayleigh waves do not produce any effect for directions more than 45° away from the surface.

Let us fix the angle θ and vary λ from zero to infinity to trace the behavior of the MS and its contribution to the displacement. We start with $\theta < 45°$ (closer to the vertical axis). In the real space, this corresponds to moving along the red line marked as "$\theta < 45°$" in Fig. 2. The motion is from outside to the origin of the coordinate system. The set of diagrams in Fig. 3 shows the dynamics of the MS and of the integration contours in the complex z-plane, where $\mathrm{Re}[z] = x$ for positive $\mathrm{Re}[z]$. The left column is for the integral J_l, the right column is for the integral J_t. The parts of the contours shown in the figure consist of horizontal and vertical cuts. The cuts at $\mathrm{Re}[z] \to \infty$ are closed by a circle of an infinite radius $|z| \to \infty$, where the integrands vanish. In each column, the upper graph serves as a reference, showing the locations of the three FS: two branch points $x = 1$ and $x = C_1$ marked as red circles, and the Rayleigh pole $x = C_2$ marked as a red cross. They are fixed, and always remain the same for the whole discussion below. As we can see from Eq. (19), for small λ all MS are on the real axis. Furthermore, from the definitions of N_l and N_t (18) we see that the singularities a_+ and b_+ appear, respectively, only when $\lambda > \sin\theta$ and $\lambda > \sqrt{C_1}\sin\theta$. Hence, for small $\lambda < \sin\theta$ the only MS are $a_- < 1$ and $1 < b_- < C_1$. When λ increases, they start moving in negative-x direction. When $\lambda = \sin\theta$, a_+ appears on top of $x = 1$, and when $\lambda = \sqrt{C_1}\sin\theta$, b_+ appears on top of $x = C_1$, but these events do not result in any special behavior of the integrals J_l and J_t. With further increase of λ the points $a_\pm$ and $b_\pm$ move to the left, and a_+ moves faster than a_-, and b_+ moves faster than b_-. At $\lambda = 1$, a_+ overtakes a_-, and their real parts become equal [see expression (19) for $a_\pm$]. At this moment a new pole appears in the integrand of J_l as shown at the graph labelled (a). Note that $\lambda = 1$ corresponds to the arrival of the longitudinal waves to the observation point. With further increase of λ the branch points $a_\pm$ form a "vertical pair" and move away from x-axis into the complex plane. This "vertical pair" moves to the left, in negative-x direction, and does not play any further role. In turn, in accordance with (19), the two branch points $b_\pm$ overlap when

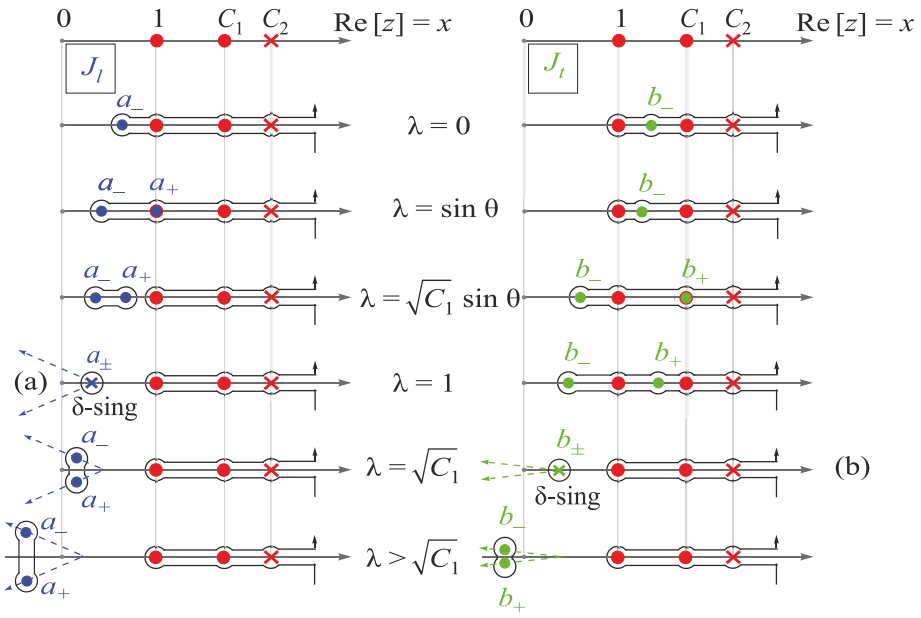

Fig. 3. (Color online) Dynamics of the moving singularities (MS) and of the integration contours with the change of λ for θ < 45°. Two large red circles and one large red cross show fixed singularities (FS) on the x-axis. Blue circles correspond to the branch points a_- and a_+ of the integral J_l, and green circles correspond to the branch points b_- and b_+ of the integral J_t. At small λ the pairs of MS approach each other on the horizontal axis as λ increases. At, respectively, λ = 1 and λ = $\sqrt{C_1}$ the pairs overlap with a formation of a new pole. These events are shown by a cross of the respective color at the plots labelled by (a) and (b) (these letters allow one to locate these events on the normal displacement snapshot (Fig. 2), where they contribute delta-singularities to U_3). With further increase of λ the pairs of MS shift into the complex plane. As λ grows, the "vertical pair" of MS shift to the left, and the vertical distance between them is growing, as shown by dotted guide-to-eye arrows in the lowest three plots.

$1 < \lambda = \sqrt{C_1}$ (graph marked as (b); $\lambda = \sqrt{C_1}$ corresponds to the arrival of the transverse waves to the observation point). This introduces a new pole into the integrand of J_t, as a result J_t has a jump and U_3 has a delta-singularity at $\lambda = \sqrt{C_1}$. After that the pair $b_\pm$ leaves the real axis and forms a "vertical pair", which, similarly to $a_\pm$, continues to the left. For larger values of λ there will be no changes in the contour shape and hence no other singularities. The events (a) and (b) are marked in the sketch of U_3 (Fig. 2) on the red line "θ < 45°".

There is one more nuance that is not captured by this discussion. If θ is very close to 45°, namely, if $1/\sqrt{C_1} < \sin\theta < 1/\sqrt{2}$, then the pair $b_\pm$ forms in between the fixed branch points $x = 1$ and $x = C_1$ [this can be seen by examining the second form of $b_\pm$ given in Eq. (19)]. In this case, when the "vertical" $b_\pm$-pair starts moving to the left, it goes over the branch point $x = 1$. This happens when

$$\lambda = \lambda_1(\theta) = \sqrt{\frac{C_1\cos^2\theta - 1}{\cos^2\theta - \sin^2\theta}}, \qquad (20)$$

and this line is marked as λ_1 in Fig. 2: it contributes a cusp to J_t, and hence a jump to U_3.

Now let us switch to the case θ > 45°, pick an angle and vary λ from zero to infinity. The corresponding dynamics of the MS is shown in Fig. 4, and all the events numbered there as (c)–(i) are marked in Fig. 2 on the red line "θ > 45°". Here a_- and b_- both form to the left of $x = 1$ and start moving to the left when λ increases. When they reach $x = 0$, they "reflect" from the origin and start moving back to the right, where they will meet, respectively, a_+ (which appears on top of $x = 1$ when $\lambda = \sin\theta$) and b_+ (which appears on top of $x = C_1$ when $\lambda = \sqrt{C_1}\sin\theta$). The points $a_\pm$ meet at $x < 1$ and produce a new pole when $\lambda = 1$ (arrival of the longitudinal wave, same as for θ < 45°), which results in a delta-singularity of the displacement component; this event is labelled as (c). After that, $a_\pm$ form a "vertical pair", which starts moving to the right, and passes over all the three FS. The same does the pair $b_\pm$. The dynamics of the MS follows the scenario outlined below. First, the "vertical" $a_\pm$-pair crosses the branch point $x = 1$ [event (d)], which happens at

$$\lambda = \lambda_2(\theta) = \frac{\sin\theta}{\sqrt{\sin^2\theta - \cos^2\theta}} \qquad (21)$$

which results in a cusp of J_l, and hence in a jump of U_3. The "vertical pair" $a_\pm$ proceeds to the right for $\lambda > \lambda_2$, and at $\lambda = \sqrt{C_1}$ b_- and b_+ overlap [event (e), arrival of the transverse wave to the observation point]. This new pole in J_t results in a delta-singularity for U_3. After that, $b_\pm$ form a "vertical pair", which passes over the fixed branch point $x = C_1$ [event (f)] at

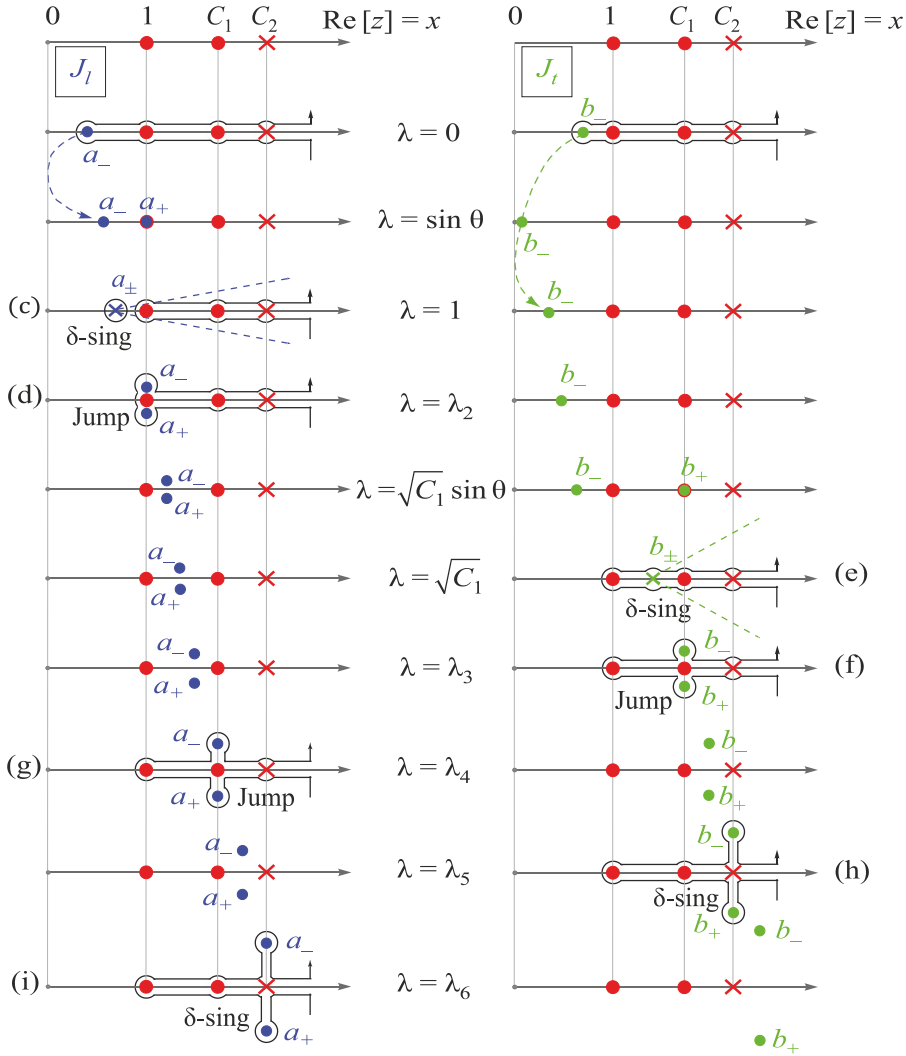

Fig. 4. (Color online) Dynamics of the MS with the change of λ for θ > 45°. The notations are the same as in Fig. 3, integration contours are shown for the most important events. After formation of the new poles in the diagrams (c) and (e), the "vertical pair" of MS move in the positive direction of the x-axis passing over all the FS. Passing of a "vertical pair" over a fixed branch point [events (d), (f), (g)] contributes a jump, and it's passing over the Rayleigh pole [events (h) and (i)] contributes a delta-singularity to U_3. The functional forms of λ_i, i = 2...6 are given in the text.

$$\lambda = \lambda_3(\theta) = \frac{\sqrt{C_1}\sin\theta}{\sqrt{\sin^2\theta - \cos^2\theta}}, \tag{22}$$

and soon after that the "vertical" $a_{\pm}$-pair passes over $x = C_1$ [event (g)] at

$$\lambda = \lambda_4(\theta) = \sqrt{\frac{C_1 - \cos^2\theta}{\sin^2\theta - \cos^2\theta}}. \tag{23}$$

Events (f) and (g) result, respectively, in cusps of J_t and J_l, and hence contribute two jumps to the displacement U_3. Finally, the "vertical pair" $b_{\pm}$, and soon after that the "vertical pair" $a_{\pm}$, pass over the Rayleigh pole $x = C_2$ [events (h) and (i)]. Each of these events adds a jump to the integral J_t or J_l, introducing two additional delta-singularities to the normal displacement. These two delta-singularities are contributions of the surface Raleigh waves, and they occur, respectively, at

$$\lambda = \lambda_5(\theta) = \sqrt{\frac{C_2 - C_1\cos^2\theta}{\sin^2\theta - \cos^2\theta}}, \qquad \lambda = \lambda_6(\theta) = \sqrt{\frac{C_2 - \cos^2\theta}{\sin^2\theta - \cos^2\theta}}. \tag{24}$$

Finally, we report the expressions for the jumps of the integral J_l

$$J_l(\lambda = 1+0, \theta) - J_l(\lambda = 1-0, \theta) = 2\pi\cos^2\theta \left(\frac{2x - C_1}{\tilde{r}(x)}\right)_{x=\sin^2\theta} \tag{25}$$

and of the integral J_t

$$J_t(\lambda = \sqrt{C_1} + 0, \theta) - J_t(\lambda = \sqrt{C_1} - 0, \theta) = \\ = \frac{16\pi \sin^4\theta \cos^2\theta(\sin^2\theta - 1/C_1)}{(2\sin^2\theta - 1)^4 + 16\sin^4\theta\cos^2\theta(\sin^2\theta - 1/C_1)}. \quad (26)$$

In [1] we discussed in detail the normal displacement in two limiting cases: at the vertical axis ($\theta = 0$) and on the surface ($\theta = \pi/2$). At the vertical axis, the displacement had only one delta-singularity at $x_3 = c_l t$. Indeed, as Eq. (26) shows, the jump of J_t is zero for $\theta = 0$, hence $\phi(\lambda, \theta = 0)$ (15) has no jump at $\lambda = \sqrt{C_1}$, and thus the delta-singularity at $x_3 = c_t t$ is suppressed (we showed in [1] that it gets replaced by a weaker singularity, a jump). This suppression is marked by an empty circle (1) in Fig. 2. This special behavior of the displacement vector is a result of the fact that at $\theta = 0$ we have $a_+ \equiv a_-$, $b_+ \equiv b_-$, and instead of a pair of branch points at all values of λ we have two poles, $a_\pm$ and $b_\pm$.

Furthermore, at the surface the displacement had no delta-singularities at all. This is consistent with Eqs. (25, 26), which state that the jumps of both J_t and J_l are zero at $\theta = \pi/2$, so the function $\phi(\lambda, \theta = \pi/2)$ has no jumps. In [1] we showed that, instead, the displacement is finite at $r_\parallel = c_l t$ and has a jump at $r_\parallel = c_t t$ [these points are marked as empty circles (2) and (3) in Fig. 2]. The third delta-singularity at the surface is expected at $r_\parallel = c_t \xi t$, where two lines of delta-singularities, $\lambda_5(\theta)$ and $\lambda_6(\theta)$, meet. The overlap of these singularities, however, leads to a different type of singularity [1], and at $r_\parallel = c_t \xi t$ the displacement diverges as $(r_\parallel^2 - (c_t \xi t)^2)^{-3/2}$, as marked by the empty circle (4) in Fig. 2.

Finally, according to (26), there is one more angle, $\sin\theta = 1/\sqrt{C_1}$, where the second jump vanishes, and the corresponding delta-singularity is suppressed. This point (marked as (5) in Fig. 2) lies at the intersection of the loci of the jump λ_1 and the second delta-surface $\lambda = \sqrt{C_1}$. Here, again, an overlap of two singularities results in a different behavior of the normal displacement.

3. Elastic energy radiated due to collision

3.1. Elastic energy due to a point surface force

In this section, we will use the expression for the normal component of the Green's function to determine the elastic energy of sound waves excited in a half-space due to an external load. In the absence of volume forces the elastic energy flow through a closed surface S is given by [3]

$$\frac{d\varepsilon}{dt} = \int_S \frac{\partial u_i}{\partial t} \sigma_{ik}\, ds_k, \quad (27)$$

where u_i are the components of the displacement vector in the medium, and $d\mathbf{s}$ is an area vector directed outwards.

We start with the energy flow caused by a normal instant point surface force $\mathbf{F} = (0; 0, F\delta(\mathbf{r}_\parallel)\delta(t))$. The surface S in Eq. (27) consists of a hemisphere with a radius $R_S \to \infty$ and a circle ($r_\parallel < R_S, x_3 = 0$). Since for any given time t we can choose such a radius R_S that the hemisphere will be ahead of the wavefront, we only need to account for the $x_3 = 0$ part of the surface. The components of the stress tensor at $x_3 = 0$ are defined by Eqs. (3), and after integrating over time we find that the elastic energy, ε_G, in this case is

$$\varepsilon_G = -F \left.\frac{\partial U_3(r_\parallel, x_3; t)}{\partial t}\right|_{r_\parallel = 0,\, x_3 = 0;\, t = 0}. \quad (28)$$

Using the second of Eqs. (5) for the displacement vector U_3, we get after converting the integration over $-\infty < \omega < \infty$ into the integral over $\omega > 0$:

$$\varepsilon_G = -\frac{2F^2}{\rho c_t^4 (2\pi)^2} \operatorname{Im} \int_0^\infty d\omega\, \omega^3 \int_0^\infty \frac{dk_\parallel\, k_\parallel \alpha_l}{r(k_\parallel^2)}. \quad (29)$$

We split the integration over $k_\parallel$ into three intervals according to different combinations of the types of waves that comprise the signal [see Fig. 1(a)], and rewrite the integrand using the dimensionless variable x defined in (11). We get:

$$\varepsilon_G = \frac{F^2 c_l}{\rho c_t^4 (2\pi)^2} \left[Q_1^{(G)} + Q_2^{(G)} + Q_3^{(G)} \right] \int_0^\infty d\omega\, \omega^2, \quad (30)$$

where the three Q-coefficients

$$Q_1^{(G)} = \int_0^1 q_1(x)\, dx, \quad q_1(x) = \frac{\sqrt{1-x}}{(2x - C_1)^2 + 4x\sqrt{(1-x)(C_1 - x)}}, \\ Q_2^{(G)} = \int_1^{C_1} q_2(x)\, dx, \quad q_2(x) = \frac{4x(x-1)\sqrt{C_1 - x}}{(2x - C_1)^4 + 16x^2(x-1)(C_1 - x)}, \\ Q_3^{(G)} = \frac{\pi}{4} \frac{\sqrt{C_2 - 1}(2 - \xi^2)^2}{C_1\xi^4 - 2\xi^2(3C_1 - 2) + 6(C_1 - 1)} \quad (31)$$

correspond to the three $k_\parallel$-intervals from Fig. 1(a). They determine how the elastic energy splits between various types of waves. Figure 5 shows the normalized coefficients $\tilde{Q}_i^{(G)} = Q_i^{(G)} / \sum_j Q_j^{(G)}$ as functions of the ratio $0 < c_t/c_l < 1/\sqrt{2}$. It is seen that the largest part of the energy is always carried away by the surface waves, while the role of the volume waves is relatively low. Note that the value of Q_3 comes entirely from the contribution of the Rayleigh pole of the corresponding real-valued integral.

The unphysical divergence of the integral over ω in (30) is due to the fact that the Fourier transform of the instantaneous force is constant. As we show in the next Subsection, for a distributed load the Fourier coefficient $\sigma_{33}(k_\parallel, \omega \to \infty) \to 0$, which provides convergence of the integral over ω.

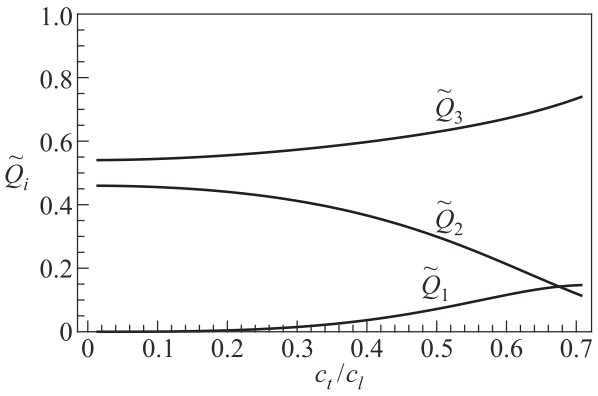

Fig. 5. The coefficients $\tilde{Q}_i = Q_i / \sum_j Q_j$ as a function of c_t / c_l.

These coefficients determine the fraction of elastic energy carried away by volume waves [$i = 1$, interval I from Fig. 1(a)], mixed volume-surface waves ($i = 2$, interval II), and pure surface waves ($i = 3$, interval III).

3.2. Collision between a small elastic ball and a large elastic object

We now switch to the case when the external force $\mathbf{F} = (0;0,F(r_\parallel,t))$ is still normal to the surface and symmetric about the x_3-axis, but is time- and position-dependent. The displacement vector now can be expressed in the form

$$u_3(\mathbf{r}_\parallel,x_3;t) = \\ = \int_0^{2\tau} dt' \int_{r_\parallel'<a(t')} d\mathbf{r}_\parallel' \sigma_{33}(\mathbf{r}_\parallel',x_3=0;t')\, U_3(\mathbf{r}_\parallel-\mathbf{r}_\parallel',x_3=0;t-t'), \tag{32}$$

where 2τ is the total time during which the force is acting, $a(t)$ is the time-dependent radius of the area where the force is applied, and $U_3(\mathbf{r}_\parallel,x_3;t)$ is the Green's function defined in (5). As before, the boundary condition is $\sigma_{33}(r_\parallel,x_3=0;t) = F(r_\parallel,t)$. Then Eq. (27) gives:

$$\varepsilon = \frac{i(2\pi)^3}{\rho c_t^4} \int_{-\infty}^{\infty} d\omega\, \omega^3 \int \frac{d^2k_\parallel \alpha_l(k_\parallel,\omega)}{r(k_\parallel^2)} \left|\sigma_{33}(k_\parallel,\omega)\right|^2, \tag{33}$$

where

$$\sigma_{33}(k_\parallel,\omega) = \frac{1}{(2\pi)^3} \int_{-\infty}^{\infty} dt \int d^2r_\parallel e^{i(\omega t - \mathbf{k}_\parallel \mathbf{r}_\parallel)} \sigma_{33}(r_\parallel,x_3=0;t). \tag{34}$$

After performing the same transformations as in Sec. 3.1 we get:

$$\varepsilon = \frac{(2\pi)^4 c_l}{\rho c_t^4}\left[Q_1+Q_2+Q_3\right], \tag{35}$$

where

$$Q_1 = \int_0^1 q_1(x)\,dx \int_0^\infty d\omega\, \omega^2 \left|\sigma_{33}(k_\parallel = \sqrt{x}\omega/c_l,\omega)\right|^2,$$
$$Q_2 = \int_1^{C_1} q_2(x)\,dx \int_0^\infty d\omega\, \omega^2 \left|\sigma_{33}(k_\parallel = \sqrt{x}\omega/c_l,\omega)\right|^2, \tag{36}$$
$$Q_3 = Q_3^{(G)} \int_0^\infty d\omega\, \omega^2 \left|\sigma_{33}(k_\parallel = \omega/c_t\xi,\omega)\right|^2$$

and the functions $q_{1,2}(x)$ and $Q_3^{(G)}$ are defined in (31).

In order to proceed we need to specify the external load $\sigma_{33}(r_\parallel,x_3=0;t)$. Let us assume that the force acting on the surface of the half-space is due to a small ball of mass m_b, which collides with the elastic half-space. Then the energy expressed by (35) defines the part of the kinetic energy of the ball that will be lost to sound waves excited in the half-space.

If the speed of the ball v is much smaller than the speed of the sound waves in the medium, we can use perturbation theory assuming that $\varepsilon \ll m_b v^2/2$. Then in the zeroth order the collision is elastic. During the collision a contact spot forms, over which the force acts onto the half-space. Using energy conservation, one can determine the radius of the contact spot, $a(t)$, in the quasistatic approximation, as well as the collision time 2τ. Using these expressions, it will be possible to determine the elastic energy lost during the collision in the first order of the perturbation theory.

We performed this calculation using the results for the static contact problem of theory of elasticity (the Hertz problem; see Sec. 9 of Ref. 3 and Problem 1 therein). The pressure created by a small ball of radius R_b on the surface of a sphere of an infinite radius (a half-space) is given by

$$\sigma_{33}(r_\parallel,x_3=0;t) = \frac{3}{2}\frac{F_0}{\pi a^2(t)}\sqrt{1-\frac{r_\parallel^2}{a^2(t)}}, \tag{37}$$

where F_0 is the force with which the two objects are compressed, and the collision time is

$$2\tau = \frac{8\sqrt{\pi}\Gamma(2/5)}{5\Gamma(9/10)}\left(\frac{5m_bD}{4\sqrt{vR_b}}\right)^{2/5}, \tag{38}$$

where D is a dimensionless factor

$$D = \frac{3}{16}\frac{(1+\kappa)}{\rho c_t^2(1-c_t^2/c_l^2)}, \quad \kappa = \frac{E}{E_b}\frac{1-\sigma_b^2}{1-\sigma^2}, \tag{39}$$

with E and σ being, respectively, the Young module and the shear module (the subscript "b" refers to the material of the ball, while its absence to the material of the half-space). This problem has been solved in [2] for the case when the ball and the half-space are made from the same material, and here we report the result for arbitrary material parameters.

We see that the coefficients (36) differ from the corresponding coefficients for the Green's function (31) only by the factor $\sigma(k_\parallel, \omega)$ replacing $F/(2\pi)^3$. The calculation showed (see [2]) that this factor depends not on $k_\parallel$ and ω per se, but on dimensionless combinations: $|\sigma_{33}(k_\parallel a_{\max}, \omega h_{\max}/v)|^2$, where $a_{\max}$ and $h_{\max} = a_{\max}^2/R_b$ are, respectively, the maximum radius of the contact spot and maximum distance of approach of the ball and the half-space (note that $h_{\max}/v \sim \tau$). Moreover, according to Eq. (36), we need to set $k_\parallel \sim \omega/c$, where c is one of the speeds of sound. Since by our assumption $v \ll c$, in the first order of perturbation theory we should keep $|\sigma_{33}(0, \omega h_{\max}/v)|^2$. Then the integrals over x and ω in (36) decouple, and the integrals over x become identical to those for the instantaneous point load, Eq. (31). The remaining integration over ω can be done analytically, and we finally obtain:

$$\varepsilon = \gamma \frac{m_b v^2}{2} \left(\frac{v}{c_t}\right)^{3/5} \left[Q_1^{(G)} + Q_2^{(G)} + Q_3^{(G)}\right], \qquad (40)$$

where

$$\gamma = \frac{100}{39\sqrt{\pi}} \frac{\Gamma(9/5)}{\Gamma(13/10)} \left(\frac{1}{10\pi}\right)^{1/5} \frac{c_l}{c_t} \left(\frac{\rho}{\rho_b}\right)^{1/5} \frac{(1 - c_t^2/c_l^2)^{6/5}}{(1+\kappa)^{6/5}} \sim 1 \qquad (41)$$

is a material-dependent factor [κ is defined in (39)]. Note that the energy split between the different types of the waves is the same as for a point source (Fig. 2).

Let us compare this result with our previous answer (30) for a point instantaneous source, where we will introduce a cut-off frequency ω_* and replace the integral with $\omega_*^3/3$. Since $F_0 = 2mv$ is the momentum transferred to the half-space, we get using Eq. (38):

$$\omega_* \sim \left(\frac{v}{c_t}\right)^{1/5} \frac{c_t}{R_b} \sim \frac{1}{\tau}. \qquad (42)$$

Then the characteristic excited wavelength is

$$\lambda_* \sim \frac{c_t}{\omega_*} \sim R_b \left(\frac{c_t}{v}\right)^{1/5} \gg R_b. \qquad (43)$$

In our calculation we accounted for the waves excited in the half-space, but neglected the vibrations of the small ball. Eq. (43) substantiates this assumption, since the vibrations with the characteristic wavelength λ_* merely do not fit into the ball. Furthermore, this inequality explains why in the first order of the perturbation theory we were able to replace $k_\parallel$ by zero in the integrands of Eq. (36). Indeed, the only parameter of the dimension of the length in our problem is R_b. Since $\lambda_* \gg R_b$, the corresponding characteristic wave vectors $k_* \sim 1/\lambda_* \ll 1/R_b$. Finally, Eq. (43) allows us to estimate the minimum linear size of the object with which the ball collides. The linear size L of the object can be neglected and the object can be modelled by a half-space if

$$L \gg \lambda_* \sim R_b \left(\frac{c_t}{v}\right)^{1/5}. \qquad (44)$$

4. Concluding remarks

The results of the last section were summarized by A. Yu. Grosberg and M. I. Kaganov in their paper in the popular science magazine "Kvant" [7]. Each of the two authors had their own history with this problem, and wanted to make the answer accessible to younger readers. Moreover, they discussed how the elastic energy emitted during a collision of two balls of a similar radii R_b (smaller than the characteristic wavelength of the sound waves) would look like. They argued that in this case

$$\varepsilon \sim mv^2 \exp\left[-\alpha \frac{\tau}{R_b/c}\right] \sim mv^2 \exp\left[-\beta \left(\frac{v}{c}\right)^{1/5}\right], \qquad (45)$$

where α and β are some numerical coefficients, and c is a characteristic speed of sound.

We would like to conclude with a quote from the introduction to that paper. After telling the reader how this problem appeared in his life and about transferring it to us, M. I. Kaganov writes: "I was happy when the solution was found. It felt like I had fulfilled my duty. Though it was not me who solved the problem, I think that I can say that I also contributed something to the solution".

We think so too. In 1995 the three of us discussed publishing this work together. Musik not only suggested this problem to us, but kept asking about our progress, discussed our findings and challenging places with us, and gave us a lot of advice and guidance. We had and still have a feeling that this work would possibly not have been done (or at least would have looked strikingly different) without his continuous presence. However, when the decision was to be made, Musik said: "I never wrote anything down with a pen. Talking does not count. I cannot author this paper, you should mention me in the acknowledgements instead". Which we did, knowing about and respecting this "using or not using a pen" rule of the old school ethics. However, we would like to use this opportunity to say that we miss seeing Musik among the authors of Refs. 1 and 2.

1. I. M. Kaganova and M. L. Litinskaia, *Phys. Lett. A* **200**, 365 (1995).
2. I. M. Kaganova and M. L. Litinskaia, *Phys. Lett. A* **200**, 375 (1995).
3. L. D. Landau and E. M. Lifshitz, *Theory of Elasticity*, Pergamon Press (1989).
4. G. F. Miller and H. Pursey, *Proc. Roy. Soc. A* **223**, 521 (1954).
5. I. M. Kaganova and A. A. Maradudin, *Phys. Scripta* **1992**, 104 (1992).

6. See Eqs. (6.699.5-6) in: *Table of Integrals, Series, and Products*, I. S. Gradshteyn and I. M. Ryzhik, Academic Press (2007).
7. A. Yu. Grosberg and M. I. Kaganov, *Kvant*, No. 2 (1996) [in Russian].

Динамічні функції Гріна для пружного півпростору та втрати енергії при зіткненні

Marina Litinskaya, Inna Kaganova

Цей спеціальний випуск присвячено 100-річчю від дня народження Мойсея Ісаковича Каганова. Ця дата — також особиста подія для нас як авторів, оскільки Мойсей Ісакович (або просто «Мусик» для своїх друзів та близьких) був батьком для однієї з нас (І. К.), і дідусем для іншої (М. Л.). Крім того, ми обидві були його ученицями та, як би у спадок, займалися пошуком вирішення проблемних питань, які окреслені у цій статті. У 1949 р. Ілля Михайлович Ліфшиць був захоплений проблемою електродинамічних й пружних властивостей твердих тіл. Цей аналіз вимагав знання відповідних функцій Гріна. Він запропонував своїм аспірантам, Мойсею Каганову та Віктору Цукернику, обчислити вектор зміщення, який викликаний точковим джерелом, що миттєво діє на поверхні пружного півпростору. Але тоді вони займалися розробкою іншої теми, та це дослідження не розглядалося до початку 1990-х років, коли М. І. Каганов запропонував цю ідею як тему магістерської роботи для однієї з нас (М. Л.), яка буде проводитися під керівництвом іншої (І. К.). Результати опубліковано у статтях I. M. Kaganova and M. L. Litinskaia, *Phys. Lett. A* **200**, 365 (1995) [1] та I. M. Kaganova and M. L. Litinskaia, *Phys. Lett. A* **200**, 375 (1995) [2]. У першій статті обговорювалося походження нормальної складової вектора зміщення. Показано, що зсув може бути обчислено як інтеграл в комплексній площині, при цьому можна вивчати зміщення як на поверхні півпростору, так і в напрямку, нормальному до поверхні. Виявлено, що особливості зміщення пов’язані з певними змінами форми контуру інтегрування. У другій статті використано вираз для нормального зміщення при обчисленні пружної енергії, викликаної зовнішнім навантаженням, знайдено кількість енергії, що втрачається маленькою кулькою, яка падає на поверхню пружного півпростору. У даній роботі розширено аналіз з урахуванням особливості вектора зміщення в довільній точці півпростору та зроблено короткий огляд наших попередніх результатів.

Ключові слова: функції Гріна, пружний півпростір, вектор зміщення, форма контуру інтегрування.